Fast Computation of the Autogram for the Detection of Transient Faults

Fast Computation of the Autogram for the detection of transient faults

Alessandro Paolo Daga[1[0000-0002-5341-7710]], Alessandro Fasana[1[0000-0001-5851-9890]], Luigi Garibaldi[1[0000-0001-9415-1915]], Stefano Marchesiello[1[0000-0001-6906-748X]], Ali Moshrefzadeh[1[0000-0002-2697-0334]]

[1] Politecnico di Torino, Dipartimento di Ingegneria Meccanica e Aerospaziale
C.so Duca degli Abruzzi, 24, 10129 Torino, Italy
alessandro.daga@polito.it
alessandro.fasana@polito.it
luigi.garibaldi@polito.it
stefano.marchesiello@polito.it
ali.moshrefzadeh@polito.it

Abstract. Structures and machines maintenance is a hot topic, as their failure can be both expensive and dangerous. Condition-based maintenance regimes are ever more desired so that cost-effective, reliable, and damage-responsive diagnostics techniques are needed. Among the others, Vibration Monitoring using accelerometers is a very little invasive technique that can in principle detect also small, incipient damages. Focusing on transient faults, one reliable processing to highlight their presence is the Envelope analysis of the vibration signal filtered in a band of interest. The challenge of selecting an appropriate band for the demodulation is an optimization problem requiring two ingredients: a utility function to evaluate the performance in a particular band, and a scheme to move within the search space of all the possible center frequencies and band sizes (the dyad {f,Δf}) toward the optimal. These problems were effectively tackled by the Kurtogram, a brute-force computation of the kurtosis of the envelope of the filtered signal (the utility function) of every possible {f,Δf} combination. The complete exploration of the whole plane (f,Δf) is a heavy task which compromises the computational efficiency of the algorithm so that the analysis on a discrete (f,Δf) paving was implemented (Fast Kurtogram). To overcome the lack of robustness to non-Gaussian noise, different utility functions were proposed. One is the kurtosis of the unbiased autocorrelation of the squared envelope of the filtered signal found in the Autogram. To spread this improved algorithm in on-line industrial applications, a fast implementation of the Autogram is proposed in this paper.

Keywords: Autogram, bearing diagnostics, Envelope Analysis, kurtosis, Spectral Kurtosis, Kurtogram, Fast Kurtogram.

1 Introduction

The optimization of machine maintenance regimes is currently a subject of great interest, as machines failure can be both expensive and dangerous. Important items to be monitored in industrial machines are the Rolling Element Bearings (REBs). In fact, early detection of bearing damages can avoid catastrophic accidents. Over the years, Vibration Monitoring emerged among the other condition monitoring techniques for its effectiveness, as a branch of signal processing specialized in the diagnostics of bearing damages [1].

REB damage signature in the time domain can be proved to be a series of repetitive transients: a train of impulse responses repeating with a specific frequency which depends on the defect location (either on the rolling element, outer or inner rings, or cage) [2]. The main issue with recognizing this signature directly in the time domain is that these characteristic impulse responses are very sharp, of short duration but low (variable) amplitude when compared to the background noise or other common contributions to the overall machine vibration signature (i.e., gears). They are commonly so weak that also in the frequency domain their amplitude contributions are covered by noise. Nevertheless, when such repetitive transients excite high-frequency resonances of the system, envelope demodulation performed over the resonance band of frequency can enhance the signal-to-noise ratio of the bearing-characteristic signal. This is commonly known as Envelope Demodulation or High-Frequency Resonance Technique [3].

The main challenge is then the selection of an appropriate band for the demodulation, sometimes defined as Informative Frequency Band (IFB). This can be seen as an optimization problem requiring two ingredients: a utility function to evaluate the performance in a particular band, and a scheme to move within the search space of all the possible centre frequencies and band sizes (the dyad $\{f,\Delta f\}$) toward the optimal.

Milestones for band selection are the Spectral Kurtosis (SK) [4] and the Kurtogram [5], which uses a single indicator (utility function) such as the kurtosis of the coefficients at the output of quasi-analytic filters with different central frequencies and bandwidths. Ideally, brute force could be used to compute the kurtosis at all the possible $\{f,\Delta f\}$ combinations. Nevertheless, in order to increase the numerical efficiency, discrete paving of the $(f,\Delta f)$ plane through a Multirate Filter-Bank structure was proposed, leading to the well-known Fast-Kurtogram (FK) [6].

Even if the FK is still a reference for bearing diagnostics, over the years many improvements were proposed. In particular, the scientific community focused on two FK weaknesses:

- The discrete paving partitioning could be improved in terms of clearer band separation and in terms of a more flexible band-limits selection
- The kurtosis is vulnerable to non-Gaussian noise so that better indicators can be taken into account.

For example, in [7] a Genetic Algorithm is used to optimize the Finite Impulse Response (FIR) filter parameters to find the optimal $\{f,\Delta f\}$ against a kurtosis-based utility function. In [8] on the contrary, the FIR filter is replaced by the Wavelet Packet Transform (WPT) to enhance the band separation.

Nevertheless, these improvements sacrifice part of the computational efficiency which was so appreciated in the original FK for an increase in the effectiveness which can be marginal. In fact, the most interesting results in improving the FK derive from the definition of better indicators generated by taking into account the nature of the bearing characteristic signal.

For example, the indicator of the Kurtogram (i.e., the time-based kurtosis) fails because the value of kurtosis, in general, decreases when the transients' repetition rate increases [9]. Hence, in [10] it is proposed to compute the kurtosis directly on the amplitudes of the envelope spectrum of the demodulated signal rather than on the filtered time signal, as this can be an indicator of "protrusion" which better depict the bearing-characteristic signal. This frequency-domain method called Protrugram has the ability to detect transients with smaller signal-to-noise ratio compared to FK, as the effect of time-domain outliers is made milder. Similarly, in [11] the kurtosis of the power spectrum of the envelope of the Wavelet Packet Transform (WPT) filtered signal is proposed.

Differently from protrusion, a measure of spectral sparsity (i.e., the ratio of L2 and L1 norm of the Squared Envelope Spectrum - SES) is used in [12] to define the Sparsogram. Spectral L2/L1 norm is studied in deep in [13] to explain the close link of SK with the spectral squared L2/L1 norm, as well as the link of L2/L1 norm with the Spectral Correlation (SC) [14].

The SC and the Cyclic Modulation Spectrum (CMS) [15] are two key approaches for Cyclic Spectral Analysis (CSA) [16], which is a family of bearing diagnostics techniques providing bispectral maps with carrier and modulation frequencies. Due to high computational costs, this family became attractive mainly after [17], where a fast estimator of SC (Fast-SC) was described by a generalization of the CMS algorithm. Anyway, it opened the field to further algorithms exploiting the relationship between cyclostationarity and envelope analysis such as the envelope-based cyclic periodogram [18] or the log-cycligram [19], as log-envelope indicators proved to be robust indicators of cyclostationarity in the case of highly impulsive noise [20]. Notice that such statistically optimal indicators of cyclostationarity are targeted methods, requiring assumptions about the periodicity of fault symptoms in the signal, and are then not "blind" as the original kurtogram.

Many other different indices, often derived by other fields, can be found in the literature to blindly improve the kurtogram. It is the case of the Gini index, an economic measure of wealth inequality (or sparseness – similarly to the idea of spectral L2/L1 norm [21]), introduced to improve the resistance of the kurtogram to noisy random impulses [22]. The infogram, based on negentropy, was instead derived from physics [23] to characterize both time-domain impulsiveness (negentropy of the Squared Envelope) and frequency-domain impulsiveness (negentropy of the Squared Envelope Spectrum), later averaged to characterize both the impulsive and cyclostationary signatures of the repetitive transients. Finally, the Correlated Kurtosis (CK) was also proposed to substitute the traditional kurtosis [24], which is usually more sensitive to a single impulse rather than the repetitive impulses typical of the bearing signature [25]. CK anyway, requires the use of the periodicity of the impulses as input information, so that it is not completely blind.

A method which is blind but takes advantage of the cyclostationarity of the signal in a different way is the Autogram [26]. In this case, the kurtosis is not computed on the squared envelope itself, but on the unbiased autocorrelation of the squared envelope of the filtered signal, so as to overcome the lack of robustness to non-Gaussian noise of the traditional Kurtogram. Because of this, a fast implementation of such Autogram is here proposed to help spreading its use.

2 The Autogram and the fast-Autogram

The Autogram finds its root in cyclostationarity. The characteristic signals from damaged bearings, in fact, are commonly considered pseudo-cyclostationary of order 2, meaning that the second order statistics (i.e., the autocovariance) is in first approximation periodic. This translates into a periodic envelope signal. In order to enhance such periodicity, the unbiased autocorrelation (AC) is then proposed. In addition, this has also the benefit of removing uncorrelated components of the signal (i.e., noise and random impulsive contents unrelated to bearing faults), ensuring robustness to Gaussian and non-Gaussian noise.

The algorithm for computing the Autogram is reported in the next section, so as to be easily compared with the proposed fast-Autogram.

2.1 The Autogram

The Autogram can be summarized by three fundamental steps [26]:

a) Split the signal in frequency bands using a dyadic tree structure by means of the wavelet transform (WT). In particular, the Maximal Overlap (undecimated) Discrete Wavelet Packet Transform (MODWPT) was used to avoid the downsampling.
b) Compute the unbiased autocorrelation (AC) of the squared envelope for each band.
c) Compute the utility function: the kurtosis of the ACs is calculated to generate a colormap able to visually highlight the bands with maximum utility.

Once the maximization is performed, the Fourier transform of the squared envelope (SES) is used to perform the demodulation and highlight the fault characteristic frequency.

2.2 The fast-Autogram

In order to improve the computational efficiency of the algorithm, it is proposed to substitute the MODWPT of the first step with the faster Multirate Filter-Bank (MFB) structure involved in the well-known Fast-Kurtogram algorithm [6]. This not only ensures a lower complexity of the paving (of the order $O(N \log N)$), but also provides better coverage of the $(f,\Delta f)$ plane. The DWPT in fact is limited to a binary subdivision, while the MFB structure can easily implement binary-ternary paving. Furthermore, the frequency localisation of the DWPT is generally poor and worsen when

progressing through the decomposition levels because of the inherent spectral aliasing [6], so that the MFB can be considered superior also in terms of performances. The fundamental steps can be then summarized as:

a) Split the signal in frequency bands using a dyadic-ternary tree structure by means of the Multirate Filter-Bank (MFB) proposed in [6].
b) Compute the unbiased autocorrelation (AC) of the squared envelope for each band.
c) Compute the utility function: the kurtosis of the ACs is calculated to generate a colormap able to visually highlight the bands with maximum utility.

Again, the Squared Envelpe Spectrum (SES) of the band showing maximum kurtosis of the ACs will be analyzed looking for the bearing characteristic spectral lines which point to damage.

In the next section, the fast Autogram performances will be compared to the Autogram and the fast-Kurtogram on the Case Western Research University (CWRU) bearing data center [27] which has become a benchmark for bearing diagnostics [28].

3 Comparison over experimental data from CWRU bearing data center

The Case Western Research University (CWRU) test rig consists of a 2 hp Reliance Electric motor driving a shaft on which a torque transducer and encoder are mounted, as shown in Fig. 1.

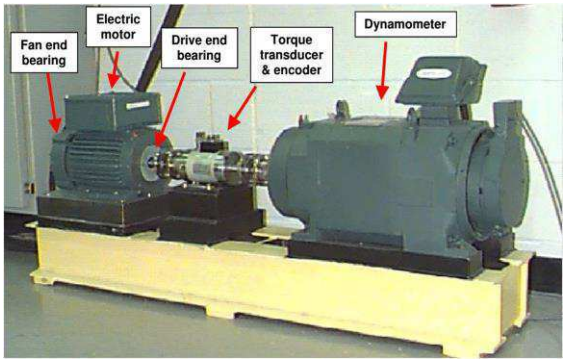

Fig. 1. CWRU bearing test rig [27,28].

Faults ranging in diameter from 0.007 to 0.028 inches (0.18 to 0.71 mm) were seeded on the rolling elements and on the inner and outer races of the drive- and fan-end bearings (described in Table 1) of the motor using electro-discharge machining (EDM). Acceleration was always measured in the vertical direction on the housing of the drive-end bearing (DE), and sometimes also in the vertical direction on the fan-end bearing housing (FE) and on the motor supporting base plate (BA). The sample rates used were 12 kHz for some tests and 48 kHz for others. The machine was then run at a constant speed for motor loads of 0 to 3 Hp (approximate motor speeds of

1797 to 1720 rpm). The complete database is quite large, and a full exploration is out of the scope of this paper. Just a small selection of acquisitions of interest, summarized in Table 2, will be analyzed. Their corresponding raw time series are reported in **Fig. 2**. For further details refer to [27].

Table 1. Bearing details and fault frequencies (BPFI/O: inner/outer race, FTF: cage, BSF: ball).

Location	Name	Fault Frequencies (multiple of shaft speed)			
		BPFI	BPFO	FTF	BSF
Drive-End	6205-2RS JEM	5,415	3,585	0,3983	2,357
Fan-End	6203-2RS JEM	4,947	3,053	0,3816	1,994

Table 2. Selected acquisitions details (DE: Drive End, FE: Fan End, IR: Inner Race, B: ball).

Name	Code	Acc. Location	Damage Location	Damage Size	Fs	Details
IR014_2	176	FE	DE – IR	0.014”	48 ksps	Normal
IR014_1	275	DE	FE – IR	0.014”	12 ksps	Impulsive noise
IR014_3	177	FE	DE – IR	0.014”	48 ksps	Electrical noise
B021_0	222	DE	DE – B	0.021”	12 ksps	Non periodic impulses

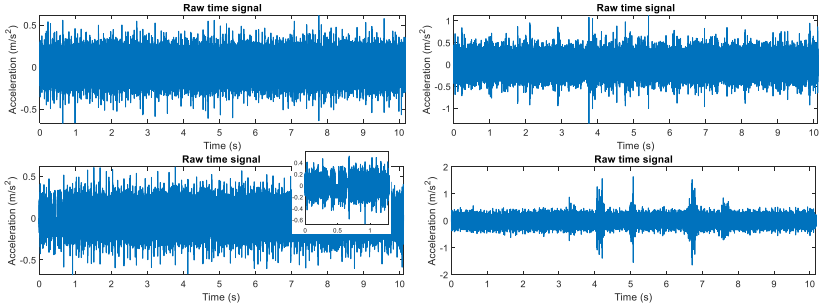

Fig. 2. Time series for the 4 cases of interest, respectively 176FE (top left), 275DE (top right), 177FE (bottom left), 222DE (bottom right).

3.1 Acquisition IR014_2 (176FE)

Acquisition IR014_2 (176FE) is selected as the first case as it is quite clean and most of the envelope-based methods are able to deal with it. The considered acceleration signal is measured on the fan-end, while a drive-end bearing damage on the inner race is present. As can be noticed in **Fig. 3**, a 7 level paving is implemented for the three algorithms, and it can be easily noticed that just a binary subdivision is used in the Autogram (A). This worsens the IFB localization in the (f, Δf) plane and explains the lower amplitudes for BPFI and 2xBPFI with respect to the fast-kurtogram (FK). In any case, the fast-Autogram (FA) solves this issue while being considerably faster: on an Intel i5 machine running Matlab R2018b, in fact, the Autogram takes 88,9s against the 1,46s of the FK and the 2,26s of the FA.

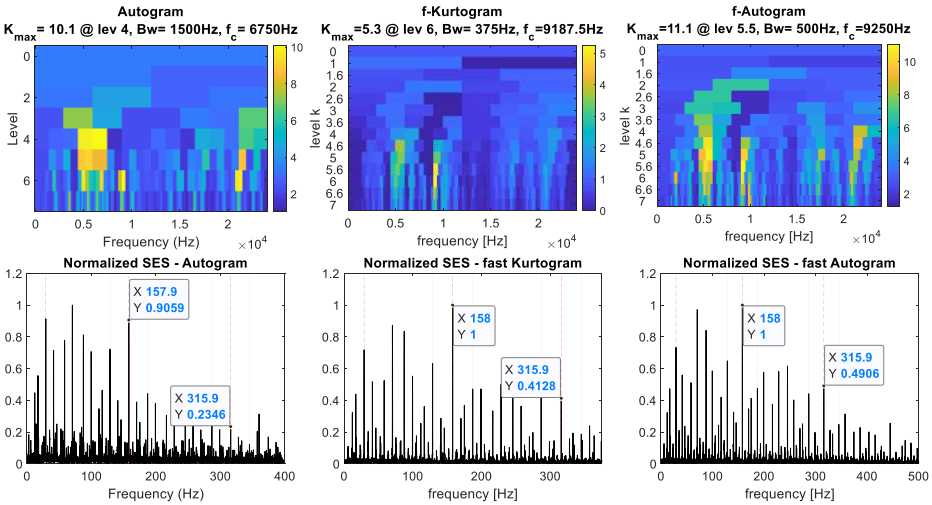

Fig. 3. Autogram, fast Autogram and fast Kurtogram with the corresponding SES of the selected band for acquisition IR014_2 (176FE). The shaft, the BPFI and 2xBPFI harmonics (DE bearing) are highlighted in the SES.

3.2 Acquisition IR014_1 (275)

Acquisition IR014_1 (275DE) is then selected. The considered measurement is the one from the drive-end accelerometer, while the fan-end bearing shows an inner race fault. As can be noticed in **Fig. 2**, this measurement involves a number of transients leading to non-stationarities which should negatively affect the FK. This is proved by the results reported in **Fig. 4**, where the SES clearly points out the superiority of the FA, whose maximum amplitude corresponds to the FE-bearing BPFI.

3.3 Acquisition IR014_3 (177)

Acquisition IR014_3 (177FE) is then considered, because of its peculiarity: it is corrupted with patches of electrical noise around 0,5s (refer to **Fig. 2**). This anomaly seems to give problems to the Multirate Filter Bank, as FK shows worst performances with respect to the Autogram. The FA is also affected by this issue but in a milder form. Both the BPFI and 2xBPFI harmonics of the DE-bearing are still visible (**Fig. 5**), proving the FA effectiveness.

3.4 Acquisition B021_0 (222DE) – Fan End bearing featuring Ball fault – Non periodic impulses

Acquisition B021_0 (222DE) is finally considered because of its highly non-stationary nature with many large impulses (**Fig. 2**). The signal measured from the DE-accelerometer was recorded with a defective DE-bearing (rolling element damage). In this case, the paving is limited to level 4 to ensure good results. Anyway, all

8

three algorithms lead to similar SES (**Fig. 6**), with visible 2xBSF harmonics. In particular, FK and FA point to the same frequency band.

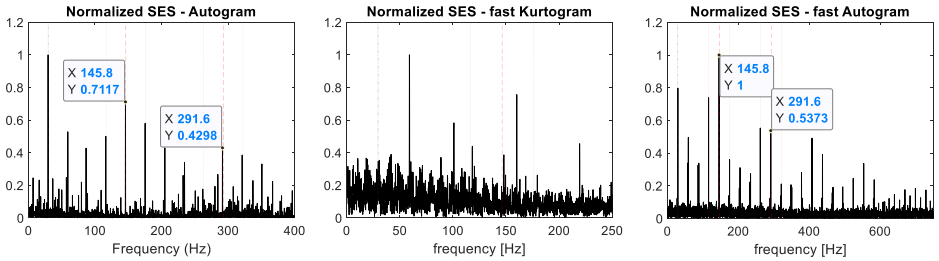

fc=1313 Hz, Bw=375 Hz T=17,1s | *fc=3625 Hz, Bw=250 Hz T=0,60s* | *fc=5625 Hz, Bw=750 Hz T=0,76s*

Fig. 4. IR014_1(275DE) - SES of the selected band (reported below the pictures) for a level 7 paving. The shaft, the BPFI and 2xBPFI harmonics (FE bearing) are highlighted. The computational times are also added.

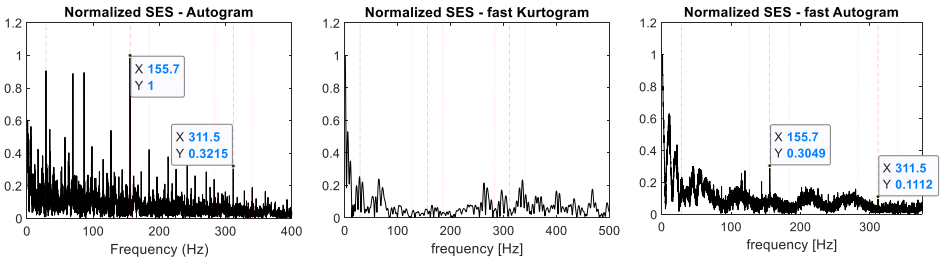

fc=18938Hz, Bw=375Hz T=42,6s | *fc=23350Hz, Bw=500Hz T=1,34s* | *fc=17813Hz, Bw=375Hz T=2,16s*

Fig. 5. IR014_3(177FE) - SES of the selected band (reported below the pictures) for a level 6 paving. The shaft, the BPFI and 2xBPFI harmonics (DE bearing) are highlighted. The computational times are also added.

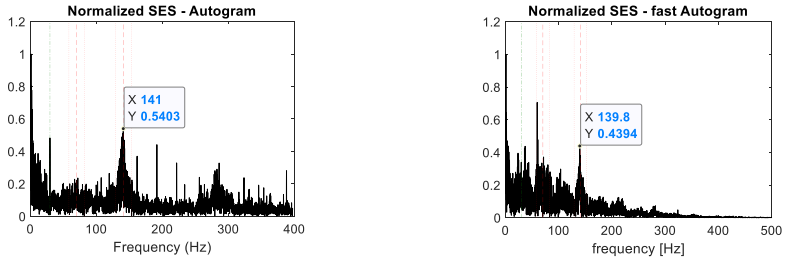

fc=3938Hz, Bw=375Hz T=2,94s | *fc=5750Hz, Bw=500Hz T=0,46s*

Fig. 6. B021_0 (222DE) - SES of the selected band (reported below the pictures) for a level 4 paving. Left: SES from Autogram. Right: SES from FA and FK. The shaft, the BSF and 2xBSF harmonics (DE bearing) are highlighted.

4 Conclusions

The scope of this paper was to provide a fast implementation of the Autogram, an algorithm claiming to be an improved version of the Kurtogram thanks to its robustness to Gaussian and non-Gaussian noise. The work was very effective in reducing the computational times, in particular for large levels of the paving: for example, for a level 7 paving of a 10s signal sampled at 48ksps, the computational times were reduced from 88s to 2s. At the same time, the Autogram robustness was kept, as tested in the four relevant case studies. Further studies on other databases (e.g. [29] for aeronautic bearings or [30] for wind turbines bearings adding the Instantaneous Angular Speed information, as in [31]) could be added in the future for demonstrating again the goodness of the algorithm. Anyway, we hope that the fast Autogram could contribute to the advancement of the state of the art of bearing diagnostics, thanks to its theoretical motivations, its speed, and its automation (human independence e.g. [32]), that make it a good candidate for online implementation.

References

1. Randall, R.B.: Vibration-based condition monitoring: industrial, aerospace and automotive applications, 3rd ed.; John Wiley & Sons, 2011. ISBN: 978-0-470-74785-8
2. Antoni J., Randall R. B.: Rolling Element Bearing Diagnostics - A Tutorial, Mechanical Systems and Signal Processing, 25(2), 485-520, 2011. DOI: 10.1016/j.ymssp.2010.07.017.
3. McFadden, P. D. and Smith, J.D.: Vibration monitoring of rolling element bearings by the high frequency resonance technique-a review, Tribology International, 17, 3-10, 1984. DOI: 10.1016/0301-679X(84)90076-8
4. Antoni J.: The spectral kurtosis: a useful tool for characterizing non-stationary signals, Mech. Syst. Signal Process. 20, 282–307, 2006, DOI: 10.1016/j.ymssp.2010.07.017
5. Antoni, J.; Randall, R.B.: The spectral kurtosis: application to the vibratory surveillance and diagnostics of rotating machines. Mech. Syst. Signal Process. 2006, 20, 308-331. DOI: 10.1016/j.ymssp.2004.09.002
6. Antoni J.: Fast computation of the kurtogram for the detection of transient faults, Mech. Syst. Signal Process. 21,108–124, 2007. DOI: 10.1016/j.ymssp.2005.12.002.
7. Wodecki, J.; Michalak, A.; Zimroz, R.: Optimal filter design with progressive genetic algorithm for local damage detection in rolling bearings. Mech. Syst. Signal Process. 2018.
8. Lei, Y.; Lin, J.; He, Z.; Zi, Y.: Application of an improved kurtogram method for fault diagnosis of rolling element bearings. Mech. Syst. Signal Process. 2011, 25, 1738-1749.
9. Barszcz, T.; JabŁoński, A.: Analysis of Kurtogram performance in case of high level non-Gaussian noise, in: The Proceedings of the 16th International Congress on Sound and Vibration, Krakow, Poland, 5–9 July 2009.
10. Barszcz, T.; JabŁoński, A.: A novel method for the optimal band selection for vibration signal demodulation and comparison with the Kurtogram. Mech. Syst. Signal Process. 2011, 25, 431-451.
11. Wang, D, Peter, W.T.; Tsui, K.L.: An enhanced Kurtogram method for fault diagnosis of rolling element bearings. Mech. Syst. Signal Process. 2013, 35, 176-199.
12. Peter, W.T.; Wang, D.: The design of a new sparsogram for fast bearing fault diagnosis: Part 1 of "Two automatic vibration-based fault diagnostic methods using the novel sparsity measurement–Parts 1 and 2". Mech. Syst. Signal Process. 2013, 40, 499-519

10

13. Wang, D.: Spectral L2/L1 norm: A new perspective for spectral kurtosis for characterizing non-stationary signals. Mech. Syst. Signal Process. 2018, 104, 290-293.
14. Antoni, J.: Cyclic spectral analysis of rolling-element bearing signals: facts and fictions, J. Sound Vib. 304 (3) (2007) 497–529.
15. Antoni, J., Hanson, D.: Detection of surface ships from interception of cyclostationary signature with the cyclic modulation coherence, IEEE J. Oceanic Eng. 37 (3) (2012) 478–493.
16. Antoni, J.: Cyclic spectral analysis in practice, Mech. Syst. Signal Process. 21 (2) (2007) 597–630.
17. Antoni, J., Xin, G., Hamzaoui, N.: Fast computation of the spectral correlation, Mech. Syst. Signal Process. 92 (2017) 248–277.
18. Borghesani, P.: The envelope-based cyclic periodogram, Mech. Syst. Signal Process. 58–59 (2015) 245-270. DOI: 10.1016/j.ymssp.2014.11.009.
19. Smith, W.A., Borghesani, P., Ni, Q., Wang, K., Peng, Z.: Optimal demodulation-band selection for envelope-based diagnostics: A comparative study of traditional and novel tools, Mech. Syst. Signal Process. 134, (2019). DOI: 10.1016/j.ymssp.2019.106303.
20. Antoni, J., Borghesani, P.: A statistical methodology for the design of condition indicators, Mech. Syst. Signal Process. 114, (2019) 290-327. DOI: 10.1016/j.ymssp.2018.05.012.
21. Wang, D.: Some further thoughts about spectral kurtosis, spectral L2/L1 norm, spectral smoothness index and spectral Gini index for characterizing repetitive transients. Mech. Syst. Signal Process. 2018, 108, 360-368.
22. Miao, Y.; Zhao, M.; Lin, J.: Improvement of kurtosis-guided-grams via Gini index for bearing fault feature identification. Meas. Sci. Technol. 2017, 28, 125001.
23. Antoni, J.: The infogram: Entropic evidence of the signature of repetitive transients, Mech. Syst. Signal Process. 74, (2016), 73-94. DOI: 10.1016/j.ymssp.2015.04.034.
24. Chen, X.; Zhang, B.; Feng, F.; Jiang, P.: Optimal Resonant Band Demodulation Based on an Improved Correlated Kurtosis and Its Application in Bearing Fault Diagnosis. Sensors (2017), 17, 360. DOI: 10.3390/s17020360
25. McDonald, G.L.; Zhao, Q.; Zuo, M.J.: Maximum correlated Kurtosis deconvolution and application on gear tooth chip fault detection. Mech. Syst. Signal Process. 33, (2012), 237–255. DOI: 10.1016/j.ymssp.2012.06.010.
26. Moshrefzadeh, A.; Fasana, A.: The Autogram: An effective approach for selecting the optimal demodulation band in rolling element bearings diagnosis, Mech. Syst. Signal Process. 105, (2018) 294-318. DOI: 10.1016/j.ymssp.2017.12.009.
27. Case western reserve university bearing data center website. URL: http://csegroups.case.edu/bearingdatacenter/home.
28. Smith, W.; Randall, R.B.: Rolling Element Bearing Diagnostics Using the Case Western Reserve University Data: A Benchmark Study. Mechanical Systems and Signal Processing. 64-65 (2015). DOI: 10.1016/j.ymssp.2015.04.021.
29. Daga, A.P.; Fasana, A.; Marchesiello, S.; Garibaldi, L.: The Politecnico di Torino rolling bearing test rig: Description and analysis of open access data. Mech. Syst. Signal Process. (2019), 120, 252–273.
30. Castellani, F.; Garibaldi, L.; Daga, A.P.; Astolfi, D.; Natili, F. Diagnosis of Faulty Wind Turbine Bearings Using Tower Vibration Measurements. Energies 2020, 13, 1474.
31. Daga, A.P.; Garibaldi, L. GA-Adaptive Template Matching for Offline Shape Motion Tracking Based on Edge Detection: IAS Estimation from the SURVISHNO 2019 Challenge Video for Machine Diagnostics Purposes. Algorithms 2020, 13, 33.
32. Daga, A.P.; Fasana, A.; Marchesiello, S.; Garibaldi, L.: Machine Vibration Monitoring for Diagnostics through Hypothesis Testing. Information, 10, 204 (2019).